pubs.acs.org/Biomac

Article

Increasing the Microfabrication Performance of Synthetic Hydrogel Precursors through Molecular Design

Aysu Arslan, Koen Vanmol, Agnes Dobos, Alessandra Natale, Jasper Van Hoorick, Patrice Roose, Hugues Van den Bergen, Tatevik Chalyan, Aleksandr Ovsianikov, Stefan Baudis, Vera Rogiers, Tamara Vanhaecke, Robim M. Rodrigues, Hugo Thienpont, Jürgen Van Erps, Sandra Van Vlierberghe,* and Peter Dubruel*

Cite This: *Biomacromolecules* 2021, 22, 4919–4932

Read Online

ACCESS | Metrics & More | Article Recommendations | Supporting Information

ABSTRACT: Implementation of hydrogel precursors in two-photon polymerization (2PP) technology provides promising opportunities in the tissue engineering field thanks to their soft characteristics and similarity to extracellular matrix. Most of the hydrogels, however, are prone to post-fabrication deformations, leading to a mismatch between the computer-aided design and the printed structure. In the present work, we have developed novel synthetic hydrogel precursors to overcome the limitations associated with 2PP processing of conventional hydrogel precursors such as post-processing deformations and a narrow processing window. The precursors are based on a poly(ethylene glycol) backbone containing urethane linkers and are, on average, functionalized with six acrylate terminal groups (three on each terminal group). As a benchmark material, we exploited a precursor with an identical backbone and urethane linkers, albeit functionalized with two acrylate groups, that were reported as state-of-the-art. An in-depth characterization of the hexafunctional precursors revealed a reduced swelling ratio (<0.7) and higher stiffness (>36 MPa Young's modulus) compared to their difunctional analogs. The superior physical properties of the newly developed hydrogels lead to 2PP-based fabrication of stable microstructures with excellent shape fidelity at laser scanning speeds up to at least 90 mm s^{-1}, in contrast with the distorted structures of conventional difunctional precursors. The hydrogel films and microscaffolds revealed a good cell interactivity after functionalization of their surface with a gelatin methacrylamide-based coating. The proposed synthesis strategy provides a one-pot and scalable synthesis of hydrogel building blocks that can overcome the current limitations associated with 2PP fabrication of hydrogel microstructures.

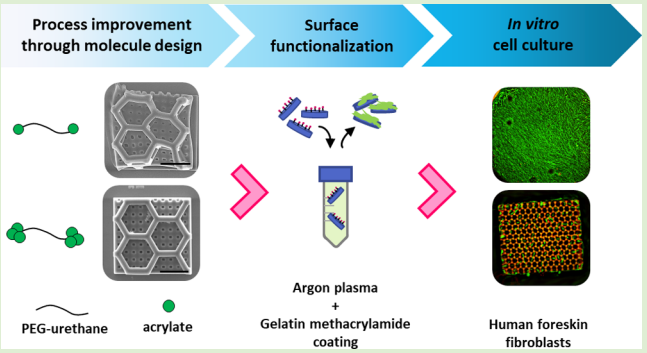

1. INTRODUCTION

With recent advances in 3D printing technologies, the production of 3D structures at the microscale range gained significant interest in tissue engineering.[1] As the natural environment of cells consists of complex 3D structures with features of different length scales, the microtopography and nanotopography of the material surface have been reported to influence cell response. Indeed, for mimicking the tissue complexity to the greatest extent possible, designing a 3D construct for tissue regeneration requires precise control over the micro- and/or nanoscale architecture.[2,3] Two-photon polymerization (2PP), also referred to as multiphoton lithography, provides an excellent methodology for generating microscaffolds with controlled dimensions at spatial resolutions down to 100 nm. The unique property of 2PP technology to elicit excellent control over scaffold architecture provides great opportunities in tissue engineering and studies concerned with unraveling cell−cell and cell−material interactions in 3D.

Although this advanced 3D printing technology offers exciting opportunities for the field of tissue engineering, its main limitation is the limited number of commercially available resins for creating suitable biomaterials for tissue engineering purposes.[4] The most commonly used resins involve low-molar-mass acrylic monomers and epoxies, which lead to highly cross-linked, nondegradable, rigid, and brittle structures that are not suitable to serve tissue engineering applications.[5,6] Conversely, hydrogel precursors form soft and flexible networks upon cross-linking. In particular, chemically cross-

Received: June 2, 2021
Revised: October 1, 2021
Published: November 1, 2021

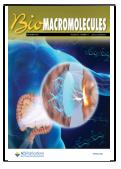

https://doi.org/10.1021/acs.biomac.1c00704
Biomacromolecules 2021, 22, 4919−4932

Table 1. List of the Synthesized Hydrogel Precursors and the Applied Reagents[a]

precursor	backbone	diisocyanate	endcapping agent	number of acrylate groups	spacer groups
UPEG-2	PEG	IPDI	OEOA	2	6 × EO
UPEG-6	PEG	IPDI	EPPETA	6	4 × EO and 1 × PO
UPEG-6-ws	PEG	IPDI	PETA	6	none

[a]PEG: poly(ethylene glycol), IPDI: isophorone diisocyanate, OEOA: oligoethyleneoxide monoacrylate, EPPETA: ethoxylated and propoxylated pentaerythritol triacrylate, PETA: pentaerythritol triacrylate, EO: ethylene oxide, and PO: propylene oxide.

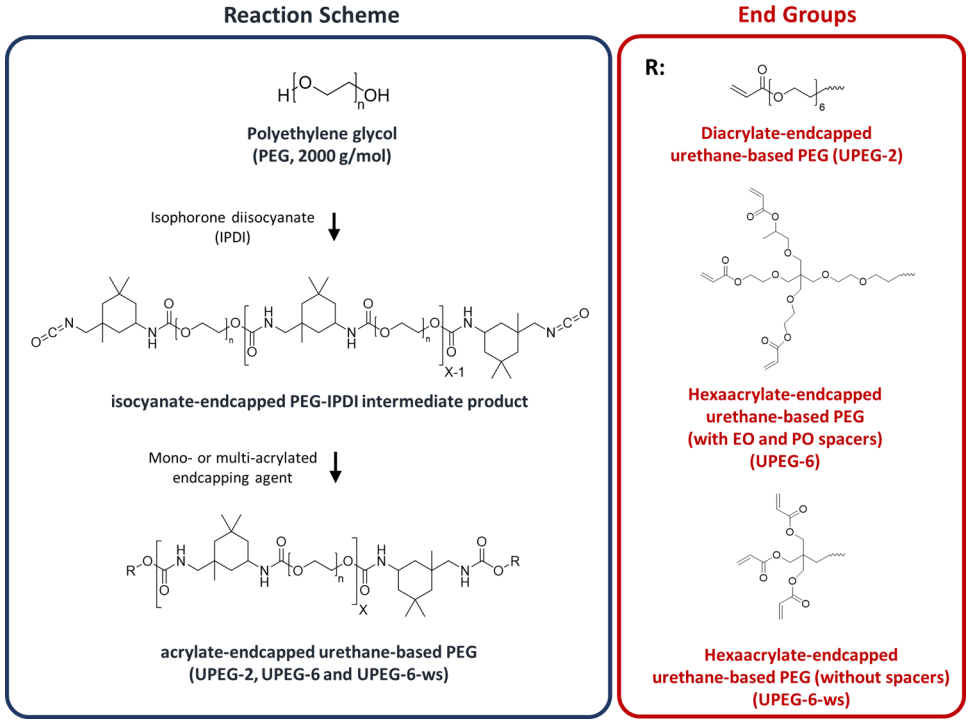

Figure 1. Reaction scheme for the synthesis of diacrylate- and multiacrylate-endcapped urethane-based PEGs exploiting endcapping agents.

linked synthetic hydrogels have become attractive alternatives for tissue engineering applications owing to their biocompatibility, tailorable design, low cost, and reproducible production routes.[7,8] In contrast to nature-derived polymers, synthetic polymers offer tunable physical properties and are compatible with various scaffold manufacturing technologies exploiting mild conditions.[8] To date, various synthetic hydrogels have been employed in 2PP fabrication of microstructures, including poly(ethylene glycol),[2,9−13] poly(2-ethyl-2-oxazolines),[14] poly(amino acids),[15] poly(vinyl alcohol),[16] and poly(glycerine).[17] Specifically, acrylate-functionalized PEGs (PEGDA) have been frequently used in multiphoton lithography due to their hydrophilicity, biocompatibility, and commercial availability. PEG is approved by the Food and Drug Administration for various applications (e.g., pharmaceuticals and wound dressings), and it can be employed as a hydrogel using a variety of cross-linking strategies, owing to its versatile macromonomer chemistry and excellent solubility in water and organic solvents.[18] However, employing PEG derivatives for the 3D fabrication of microstructures poses several challenges due to their swelling behavior and low stiffness.[19] These characteristics of the cross-linked acrylated PEG derivatives often result in structure deformation and poor control over the geometry of the microscaffold. Furthermore, realization of accurate structures becomes more challenging when the structural design has an open geometry, as the capillary forces caused by the evaporating developer lead to significant distortion or structural collapse.[20] To date, most of the PEGDA formulations applied in 2PP exploit low-molar-mass PEGs (<750 g mol^{-1}) to obtain an effective microfabrication process owing to a sufficiently high cross-linking density.[9−12,21−24] Nevertheless, it was reported that the processability of the latter is still prone to deformations associated with swelling and detachment from glass substrates.[9,19,25] Moreover, a narrow polymerization window has been observed, which limits tuning of microstructure dimensions and therefore the resolution of the printed structures.[15] Scarpa et al. investigated the 2PP processability of PEGDA with a molar mass of 10,000 g mol^{-1} for the design of bulk architectures (e.g., pyramids).[13] However, the printability of the high-molar-mass PEGDAs was not investigated to create complex and hollow architectures.

Recently, we introduced a telechelic hexaacrylate-endcapped urethane-based poly-ε-caprolactone for 2PP-based fabrication of biodegradable microstructures.[26] Upon photopolymerization, the hexaacrylate-endcapped urethane-based prepolymers form a phase-separated structure with dense cross-linking, resulting in a remarkably enhanced toughness while improving the 2PP processability compared with their diacrylate-endcapped counterparts.

In the current work, we applied a similar structural approach using a PEG backbone (2000 g mol^{-1}) with urethane linkers, in order to obtain hydrogels with superior mechanical properties for the fabrication of stable microscaffolds. To this

https://doi.org/10.1021/acs.biomac.1c00704
Biomacromolecules 2021, 22, 4919−4932

end, two different multiacrylate monomers were covalently linked as terminal groups to the PEG backbone via isophorone diisocyanate (IPDI) linkers. More specifically, pentaerythritol triacrylate (PETA) and ethoxylated/propoxylated pentaerythritol triacrylate (EPPETA) were covalently linked to the PEG-urethane backbone. The latter consists of a flexible alkoxy core (i.e., ethylene oxide and propylene oxide units) that acts as a spacer between the acrylate groups, whereas the former lacks the flexible core.

The multiacrylate-endcapped urethane-based precursors and the resulting cross-linked networks were characterized in terms of their physicochemical properties and their processing potential via 2PP. The characteristics and processing performance of the multifunctional polymers were compared to those of their difunctional analogs. Finally, the potential of the newly developed multifunctional polymers to serve tissue engineering applications was explored via a number of cell culture assays.

2. MATERIALS AND METHODS

2.1. Synthesis of Hydrogel Precursors. Hydrogel precursors were synthesized using a PEG backbone (2000 g mol^{-1}, Sigma-Aldrich), isophorone diisocyanate (IPDI, Sigma-Aldrich), and the endcapping agents monoacrylated oligoethyleneoxide (OEOA, Bisomer PEA6, GEO Specialty Chemicals), ethoxylated and propoxylated pentaerythritol triacrylate (EPPETA, Allnex), and pentaerythritol triacrylate (PETA, Allnex). Prior to the reaction, PEG was dried for 3 h by applying vacuum under a dry N_2 blanket. Subsequently, PEG was reacted with IPDI at 75 °C in a 1:2 stoichiometric ratio using 300 ppm bismuth neodecanoate (Umicore) as a catalyst in the first reaction step. The first step of the reaction was continued until 50% of the isocyanates were consumed as determined via potentiometric titration. In the second reaction step, 2 equiv. of endcapping agents was added together with 300 ppm bismuth neodecanoate and reacted at 80 °C under dry air until the residual isocyanate (NCO) value decreased below 0.02 meq g^{-1}, as determined by potentiometric titration. Finally, phenothiazine (500 ppm) and triphenyl phosphite (500 ppm) were added into the product as post-stabilizers.

All three hydrogel precursors were synthesized using the same method except for the applied endcapping agents. The endcapping agents OEOA, EPPETA, and PETA consist of 1, 3, and 3 acrylates on average, which were used in the synthesis of UPEG-2, UPEG-6, and UPEG-6-ws precursors, respectively. Both UPEG-6 and UPEG-6-ws consisted of six acrylates; however, the former contains ethylene oxide (EO) and propylene oxide (PO) spacer units linked to the acrylate groups, whereas the latter lacks spacer groups. The synthesized hydrogel precursors and the applied reagents during the synthesis are summarized in Table 1 and Figure 1.

After the synthesis, UPEG-2 precursors were used without further purification. UPEG-6 and UPEG-6-ws precursors were isolated via dialysis in acetone using a regenerated cellulose dialysis membrane tubing (MWCO of 1 kDa, Spectrum Spectra/Por) in order to remove the unreacted endcapping agents. All characterization and processing studies were performed on the isolated hexafunctional precursors unless stated otherwise.

2.2. Characterization of Chemical Structures. The chemical structures of the synthesized polymers were analyzed via Fourier transform infrared (FTIR) and proton nuclear magnetic resonance (^{1}H NMR) spectroscopy. FTIR spectroscopy was conducted on a PerkinElmer Frontier FTIR mid-IR combined with an MKII Golden Gate setup equipped with a diamond crystal from Specac, operating in attenuated total reflection (ATR) mode. Spectra of the PEG, the intermediate product of the first reaction step (PEG-IPDI), and the final products were recorded for the range of 500−4000 cm^{-1} applying eight scans.

Nuclear magnetic resonance spectroscopy analyses were performed on a 400 MHz spectrometer (Bruker Avance) at room temperature after dissolving the polymers in deuterated chloroform ($CDCl_3$, Euriso-Top) at a concentration of 10 mg mL^{-1}. The spectra were analyzed using MestReNova software (version 6.0.2). For quantification of the acrylate concentration, dimethyl terephthalate (DMT, Sigma-Aldrich) was added into the NMR solutions of the precursors at a concentration of 10 mg mL^{-1}, and the acrylate concentration was calculated using eq 1.

$$C_{acr} = \frac{I_{\delta=5.8\ ppm} + I_{\delta=6.1\ ppm} + I_{\delta=6.3\ ppm}}{I_{\delta=8\ ppm}} \times \frac{N_{H,\delta=8\ ppm}}{N_{\delta=5.8\ ppm} + N_{\delta=6.1\ ppm} + N_{\delta=6.3\ ppm}} \times \frac{W_{DMT}}{MM_{DMT}} \times \frac{1000}{W_p} \quad (1)$$

where C_{acr} is the amount of acrylates in the precursors (mmol acrylate/g precursor), ($I_{\delta\ =\ 5.83\ ppm} + I_{\delta\ =\ 6.12\ ppm} + I_{\delta\ =\ 6.30\ ppm}$) is the sum of the integrals of the signals of the protons arising from the acrylates (δ = 5.83, 6.12, and 6.30 ppm), $I_{\delta\ =\ 8\ ppm}$ is the integral of the signal of the protons characteristic of the aromatic ring in DMT (δ = 8 ppm), ($N_{\delta\ =\ 5.8\ ppm} + N_{\delta\ =\ 6.1\ ppm} + N_{\delta\ =\ 6.3\ ppm}$) is the number of protons in one acrylate end group, $N_{H,\ \delta\ =\ 8ppm}$ is the number of protons in the benzene ring of DMT, W_{DMT} corresponds to the weight of DMT, W_p is the weight of the precursor, and MM_{DMT} is the molar mass of DMT.

2.3. Determination of Molar Masses. The number average molar mass (M_n), the weight average molar mass (M_w), and the polydispersity index ($Đ$) were determined by gel permeation chromatography (GPC) using PEG standards (Agilent Technologies, weight average M_w range of 420−200.000 g mol^{-1}). The hydrogel precursors were dissolved (10 mg mL^{-1}) in chloroform (Biosolve, HPLC grade) and filtered (0.45 μm pore size) prior to analysis. Analyses were performed by liquid chromatography, using an Alliance Waters 2695 separation module with a Waters 2414 refractive index detector, equipped with a PLGel Mixed-D (particle size of 5 μm) polystyrene/divinylbenzene GPC column.

2.4. Evaluation of Photo-Cross-Linking Kinetics. The precursors were formulated with Irgacure 2959 (2 mol % with respect to the acrylate concentration) as a photoinitiator prior to the evaluation of curing kinetics via differential photocalorimetry (DPC). DPC thermograms were recorded using a Mettler DSC823e equipped with a Hamamatsu Lightningcure LC8 lamp (medium-pressure mercury−xenon lamp, with intensity adjusted to 15 mW cm^{-2} at 365 nm). All measurements were conducted using dry nitrogen as an inert flow gas (50 mL min^{-1}). Prior to irradiation, the samples were held in the molten state at 60 °C for at least 10 min under nitrogen gas flow to remove all dissolved oxygen. Next, the samples were cooled down to 20 °C at a rate of 5 K min^{-1}, equilibrated for 10 min, and subsequently exposed to UV light at 20 °C. The duration of UV exposure was 4 min. With empty crucibles, the heat flow signal generated by incident light was largely cancelled upon simultaneous illumination of the reference and the sample side of the cell. However, imperfect compensation still led to a shift of the baseline upon exposure to the light source. After suitable baseline correction, the heat flow signal was scaled by the total heat of polymerization calculated from the double bond content to obtain the conversion rate. The maximum polymerization rate R_{max} and final acrylate conversion p_f of the precursors were determined using eqs 2 and 3.

$$R_{max} = h_{max}/(C_{acr}\Delta H_o) \quad (2)$$

$$p_f = \Delta H/(C_{acr}\Delta H_o) \quad (3)$$

where h_{max} is the maximum heat flow, C_{acr} is the acrylate double bond concentration of the precursors as determined via ^{1}H NMR spectroscopy (see Table 2), ΔH is the reaction enthalpy, and ΔH_o is the molar reaction enthalpy of acrylate double bonds (77.6 ± 1.1 kJ mol^{-1}).[27]

2.5. Evaluation of the Physical Properties of the Cross-Linked Hydrogels. *2.5.1. Sample Preparation.* The hydrogel

https://doi.org/10.1021/acs.biomac.1c00704
Biomacromolecules 2021, 22, 4919−4932

Table 2. Actual and Theoretical Concentration of Acrylates (C_{acr}), Number Average (M_n) and Weight Average (M_w) Molar Masses, and Polydispersity Indexes ($Đ$) of the Acrylate-Endcapped Urethane-Based Precursors as Determined via Gel Permeation Chromatography

sample	C_{acr} (mmol g^{-1})	theoretical C_{acr} (mmol g^{-1})	M_n (g mol^{-1})	M_w (g mol^{-1})	$Đ$
PEG			2100	2200	1.04
UPEG-2	0.55	0.60	8900	13,700	1.53
UPEG-6	1.41	1.70	11,200	18,900	1.70
UPEG-6-ws	1.92	2.00	9400	14,300	1.50

precursors were formulated with Irgacure 2959 (2 mol % with respect to the acrylate concentration) as a photoinitiator prior to cross-linking. The polymer/photoinitiator blends were molten at 60 °C and placed between two glass plates separated by a 1 mm-thick silicone spacer. Next, the formulations were kept at room temperature for 10 min and were subsequently irradiated with UV-A radiation (15 mW cm^{-2}) for 30 min.

2.5.2. Swelling and Gel Fraction Tests. The UV-cross-linked hydrogels were cut into disks (D of 10 mm, triplicates) using a hollow puncher and weighed (W_i). Next, the dry gels were incubated in deionized water for 3 days at room temperature and weighed in the swollen state (W_s). Finally, the hydrogels were frozen and lyophilized to determine their final dry weight (W_d). Swelling ratios and gel fractions were determined using eqs 4 and 5, respectively.

$$\text{swelling ratio} = \frac{W_s - W_d}{W_d} \tag{4}$$

$$\text{gel fraction} = \frac{W_d}{W_i} \times 100\% \tag{5}$$

2.5.3. Tensile Tests. The cross-linked precursors were punched out into dog-bone-shaped samples (1 mm thickness, 30 mm gauge length, and 4 mm width, four replicates) and soaked in deionized water for 24 h at room temperature prior to tensile tests. Next, the equilibrium swollen hydrogels were evaluated at room temperature using a universal testing machine (Tinius Olsen) equipped with a 500 N load cell. A preload force of 0.3 N was applied, and the specimens were tested at a crosshead velocity of 10 mm min^{-1}. Young's moduli were calculated from the initial slope (<1% strain) of the stress−strain plots.

In order to estimate the toughness of the hydrated hydrogels, deformation energies were calculated from the area under the stress−strain plots using eq 6.

$$U_T = \int_0^{\varepsilon_b} \sigma \, d\varepsilon \tag{6}$$

where σ is the tensile stress, ε is the strain, ε_b is the strain at break, and U_T is the deformation energy.

2.6. Cell Culture Tests. *2.6.1. Evaluation of Indirect Cytotoxicity Using Human Foreskin Fibroblasts.* For the cell culture tests, nonpurified hydrogel precursors were used. Human foreskin fibroblasts (HFFs) (American Type Culture Collection, SCRC-1041) collected under informed consent were cultured in Dulbecco's modified Eagle's medium (DMEM) supplemented with 10% fetal bovine serum (FBS) and 1% penicillin−streptomycin solution. Upon 90% confluency, the cells were detached using Accutase solution, reseeded in T75 flasks (Greiner Bio), and maintained at 37 °C under a 95% air/5% CO_2 atmosphere. The cells were used between passages 8 and 12.

In vitro cytotoxicity of the materials was tested according to the ISO 10993-5 protocol. HFFs were detached using trypsin−EDTA and were seeded at a concentration of 5000 cells/well in a 96-well plate and were left to adhere overnight. The cross-linked hydrogel disks were sterilized by UV-C irradiation for 20 min. The extract tests were performed by incubating cross-linked hydrogel disks (surface area of 3 cm^2 mL^{-1}) in either DMEM cell culture media with 10% FBS or in dimethyl sulfoxide (DMSO) for 24 h at 37 °C. Next, the extracts were used as incubation media for HFF cells. More specifically, extracts performed in a DMEM cell culture medium were directly used as an incubation medium for HFF cells (Medium 1). However, the DMSO extraction media were further diluted to 0.5 vol % in a culture medium (Medium 2) prior to addition to the cells.

The cells were incubated in extracts (Medium 1 and Medium 2) for 24 h in a cell culture incubator before conducting 3-(4,5-dimethylthiazol-2-yl)-5-(3-carboxymethoxyphenyl)-2-(4-sulfophenyl)-2*H*-tetrazolium (MTS) assays according to the manufacturer's protocol. As a positive control, cells were incubated in an extract-free cell culture medium supplemented with FBS. As a negative control, cells were incubated in a cell culture medium supplemented with 10 vol % DMSO.

2.6.2. Evaluation of Cell Interactivity Using Human Foreskin Fibroblasts. The surfaces of the cross-linked hydrogel disks and scaffolds were functionalized prior to cell culture studies in order to improve cell−material interactions. For this purpose, X Gel-MA INX (Xpect INX), a formulation based on gelatin methacrylamide, was applied as a surface coating onto the cross-linked hydrogel disks.

Prior to coating, the cross-linked hydrogels were surface-treated using argon plasma for 10 min in order to ensure a homogeneous coating on the surface of the hydrogels. Inert gas plasmas are known to cause hydrogen abstraction followed by incorporation of oxygen on the polymer surface in the post-plasma treatment.[28] Therefore, functionalization can be anticipated on the surfaces of disks and scaffolds that have contact with the ambient atmosphere leading to an improvement of the coating. Next, the surface-treated hydrogels were incubated in a five times diluted X Gel-MA INX solution for 1 h at 40 °C. Next, the samples were removed from the coating solution, placed into a sealed bag, and flushed with argon gas. Finally, the coated hydrogels were irradiated with UV-A (15 mW cm^{-2}) for 60 min to initiate the chemical cross-linking reaction of the applied coating.

The prepared hydrogel films were sterilized for 20 min using UV-C and were subsequently immersed in phosphate buffer saline (PBS) containing 1% penicillin−streptomycin solution in a 24-well cell culture plate and placed in an incubator at 37 °C for 48 h. After that period, PBS was exchanged to FBS, and the hydrogel disks were further incubated for 1 h prior to cell seeding. Afterward, HFF cells were detached from the T75 flasks using Accutase and subsequently drop seeded onto the disks at a concentration of 5×10^4 cells per well.

For live-dead staining, calcein AM and propidium iodide (PI) (Gibco Life Technologies) were prepared in PBS according to the manufacturer's directions. The samples were stained for 30 min prior to imaging with a fluorescence microscope (Olympus IX 81, Olympus).

In order to assess the viability of the cells based on their metabolic activity, a MTS assay (Abcam) was performed. To avoid including cells growing on the outer plastic parts of the surface of the wells, the disks were placed in a new 24-well plate. Next, the MTS assay was subsequently carried out according to the manufacturer's instructions. The samples were incubated for 2 h before reading the absorbance at 490 nm using a plate reader.

2.6.3. Evaluation of Indirect Cytotoxicity Tests Using HepG2 Cells. In order to determine whether hydrogels release toxic substances in the medium, an indirect cytotoxicity test was performed using the HepG2 hepatic carcinoma cell line. Initially, the cross-linked hydrogels were sterilized by incubation in 70% (v/v) sterile ethanol (Sigma-Aldrich) for 3 h followed by irradiation with UV-C for 1 h. Next, the polymers were rehydrated in sterile PBS overnight. After swelling, the polymer sheets were cut into disks (D of 11 mm) using hollow punchers and placed in 48-well cell culture plates (Greiner Bio-One). Collagen-coated (0.1 mg mL^{-1}, Thermo Fisher Scientific) and noncoated tissue culture plates were used as controls. The polymer disks as well as the noncoated and collagen-coated controls were incubated in 1 mL of a growth medium for 72 h prior to cell seeding. The growth medium consisted of DMEM + GLUTAMAX/F12 Nutrient Mixture (3:1; Thermo Fisher Scientific), supplemented with 20% (v/v) B27 (Thermo Fisher Scientific) and 5% (v/v) FBS

https://doi.org/10.1021/acs.biomac.1c00704
Biomacromolecules 2021, 22, 4919−4932

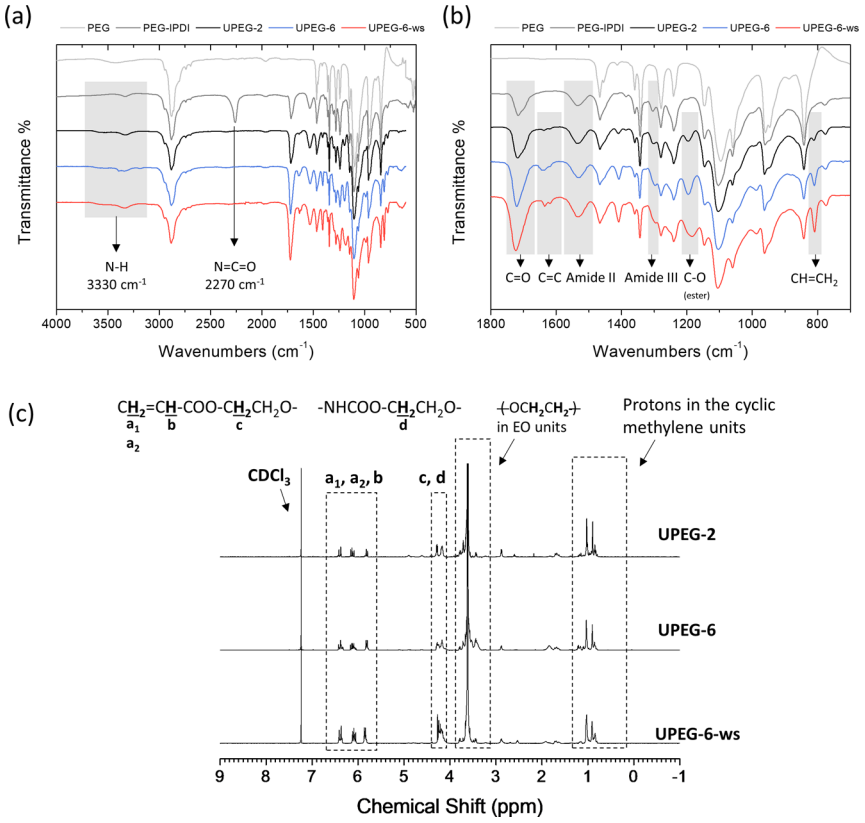

Figure 2. FTIR spectra of synthesized diacrylate- and multiacrylate-endcapped urethane-based PEGs: (a) in the region 500−4000 cm^{-1} and (b) in the region 700−1800 cm^{-1} and (c) ^1H NMR spectra of UPEG-2, UPEG-6, and UPEG-6-ws.

(Hyclone). After this period, the preincubation media of each well of the polymers from the same group were collected, pooled together, and stored at 4 °C. On the day of seeding, approximately 20,000 HepG2 cells were seeded in each well in the presence of FBS and incubated for 24 h to allow cell adherence. After 1 day, the cells were refreshed with the preincubation media (previously stored in the fridge, without FBS) of the respective polymers and cultured for one week. Cell numbers were determined on days 1, 3, and 7 of cell culture using the CellTiter-Glo Luminescent Cell Viability Assay (Promega) according to the manufacturer's instructions.

2.7. Two-Photon Polymerization Processing. The photoinitiator M2CMK[29] was dissolved in tetrahydrofuran (THF) (stock solution concentration of 7 mM). Next, hydrogel precursors were dissolved in this M2CMK stock solution in which the molar ratio between M2CMK and the acrylate groups was kept at 0.02.

After complete dissolution of the precursors in THF, 20 μL of the prepared solution was drop cast on a borosilicate glass substrate. In order to enhance the sample adhesion, the glass substrates were presilanized by immersion into a dilute solution of 3-(trimethyoxysilyl) propyl methacrylate in acetone before use. After drop casting the precursor, the solvent was evaporated for 30 min at room temperature prior to 2PP processing. After evaporation of THF, the remaining polymer on the glass substrate was processed via a commercially available 2PP system (Photonic Professional GT+, Nanoscribe GmbH) equipped with near-infrared laser light with a wavelength of 780 nm, a pulse duration of 100 fs, and a repetition rate of 80 MHz. The precursors were processed using a 63× or a 25× microscope objective with scanning speeds ranging from 10 to 90 mm s^{-1}, whereas the average laser power in the process was in the range of 5 to 50 mW. After completion of the printing process, the samples were developed upon immersion into propylene glycol monomethyl ether acetate (PGMEA) for 30 min at room temperature to remove the noncross-linked precursor.

Morphologies of the dry scaffolds were observed via scanning electron microscopy (SEM, HIROX 4500M) after sputter-coating of the scaffolds (JFC-2300, Jeol) with a gold film (thickness of about 12 nm). Additionally, the morphologies of the scaffolds prior to and after 1 h of incubation in PBS (37 °C) were monitored via an inverted microscope (Leica DMi8) using an excitation wavelength of 405 nm and a fluorescence emission range between 420 and 600 nm.

Deformation of the features of the scaffolds was estimated using eq 7.

$$X = \frac{d_t - d_a}{d_t} \times 100\% \quad (7)$$

where X is the deformation percentage, d_a is the actual length of the features, and $d_t$is the theoretical length. The actual length of the scaffold features was determined using ImageJ software (NIH, USA).

2.8. Statistical Analysis. At least triplicate samples were used for the analyses. Statistically significant differences were determined via a one-way ANOVA with Bonferroni's post hoc test (OriginPro 8.5 software). Two values were considered significantly different when $p < 0.05$. Data are expressed as the mean ± standard deviation.

3. RESULTS AND DISCUSSION

Three different acrylate-endcapped urethane-based hydrogel precursors were synthesized via a two-step urethanization reaction as schematically represented in Figure 1. The investigated polymers were based on the same PEG backbones (molar mass of 2000 g mol^{-1}) and urethane linkers albeit terminated with a different number of acrylate groups and spacers.

The endcapping agents (ECA) used herein are composed of a different number of acrylate moieties (1 versus 3) with and without spacer units. More specifically, the ECAs OEOA, PETA, and EPPETA are respectively composed of 1, 3, and 3 acrylates on average. It should be noted that the ECAs EPPETA and PETA are composed of an equal number of

https://doi.org/10.1021/acs.biomac.1c00704
Biomacromolecules 2021, 22, 4919−4932

acrylates, with the former containing an EO and PO core (i.e., spacer units) separating the photoreactive acrylate groups whereas the latter lacking spacer groups. It is hypothesized that both the presence of spacers and the number of acrylates will have a profound impact on the characteristics of the polymers such as the curing kinetics of the precursors as well as the physical properties of the cross-linked networks.[30]

3.1. Characterization of the Prepolymers. *3.1.1. Characterization of the Chemical Structures.* Fourier transform infrared (FTIR) spectra of the starting macrodiol PEG, the intermediate product resulting from the first reaction step (PEG-IPDI), and the final diacrylate- and hexaacrylate-endcapped precursors (UPEG-2, UPEG-6, and UPEG-6-ws) are shown in Figure 2a,b.

At the end of the first reaction step, the absorption bands corresponding to the N−H stretch (3330 cm^{-1}), the C═O stretch (1710 cm^{-1}), the amide II (1540 cm^{-1}), and the amide III bands (1300 cm^{-1}) could be observed in the spectrum of the intermediate PEG-IPDI product, confirming the urethanization reaction. The absorption band at 2270 cm^{-1}, characteristic of the free isocyanate groups, was also visible in the PEG-IPDI intermediate product. This absorption band disappeared completely at the end of the second reaction step, confirming that all free isocyanates were consumed at the end of the reaction for UPEG-2, UPEG-6, and UPEG-6-ws (Figure 2a).

The characteristic absorption bands arising from the acrylate functional groups are visible in the spectra of all final products. More specifically, the C═C stretch of the acrylate groups can be observed at 1635 cm^{-1}, the C−O stretch of the acrylate esters is present at 1180 cm^{-1}, and the $=CH_2$ out-of-plane deformation can be observed at 810 cm^{-1} in the spectra of UPEG-2, UPEG-6, and UPEG-6-ws (Figure 2b).

^1H NMR spectra of the products UPEG-2, UPEG-6, and UPEG-6-ws are shown in Figure 2c. The signal corresponding to the methylene protons of PEG that are adjacent to the hydroxyl functionalities shifted from around δ = 3.61 ppm to δ = 4.15 ppm as a result of the urethanization reaction. In the spectra of the final products UPEG-2, UPEG-6, and UPEG-6-ws, the signals between δ = 3.3 and δ = 3.8 ppm can be attributed to methylene protons present in the PEG backbone (for all precursors), EO spacers (for UPEG-2 and UPEG-6), and PO spacers (for UPEG-6). The signals between δ = 0.7 and δ = 2.0 ppm correspond to the protons from the cyclic methylene units of IPDI, while the signal at δ = 4.25 ppm is assigned to the $-CH_2-$ protons adjacent to the acrylate esters, and the signals at δ = 5.83, 6.12, and 6.30 ppm belong to the protons from the acrylate double bonds. The concentration of acrylates (C_{acr}) for each polymer was determined quantitatively using the NMR standard dimethyl terephthalate (DMT) and was found to be 0.55, 1.41, and 1.92 mmol g^{-1} for UPEG-2, UPEG-6, and UPEG-6-ws, respectively (Table 2).

3.1.2. Determination of Molar Mass. The molar mass of the polymers was analyzed via gel permeation chromatography (GPC), and data are presented in Table 2. The molar masses of the hexaacrylate-endcapped polymers were found to be at least three times higher than that of the starting product PEG (2000 g mol^{-1}), which can be explained through the repeating effect of PEG-IPDI. The latter effect can be explained with the use of a nonsymmetrical isocyanate (i.e., IPDI) in the synthesis of hydrogel precursors. IPDI consists of a primary and a secondary isocyanate, and the selectivity on the isocyanates of IPDI is dependent on various factors, including the catalyst type. In our study, we used a bismuth-based catalyst due to its biocompatibility.[26,31] It has been reported that the selectivity of bismuth-based catalysts over the secondary isocyanates is lower compared to the tin-based catalysts, which are frequently used in the synthesis of urethane-based polymers.[32] A decreased selectivity of the catalyst results in the reaction of a certain amount of the primary isocyanate groups of IPDI as well as the secondary isocyanate groups in the first reaction step, leading to the formation of repeating "PEG-IPDI" units, thereby increasing the molar mass.

It was observed that the hexafunctional precursors revealed a slightly higher molar mass compared to UPEG-2. This result can be explained with the structure of the multiacrylate ECAs applied in the synthesis of UPEG-6 and UPEG-6-ws. The commercially available multiacrylate ECAs consisted of a mixture of monomers, and they were used for our syntheses without further purification. Although the commercial ECAs are composed of n acrylates and one hydroxyl group on average, a certain fraction of these ECAs is composed of $n - 1$ acrylates with two hydroxyl moieties. As a result, part of the ECAs reacted with two or more PEG-IPDI units, which resulted in a slightly increased molar mass. Further, a fraction of the ECA molecules could not be covalently linked to the polymer backbone during synthesis due to the lacking hydroxyl functionality and thus remained as byproducts after the synthesis. This was evidenced by the presence of a low-molar-mass fragment in the chromatograms (Figure S1, dashed lines). In the case of UPEG-6, this fragment corresponded to the molar mass range of the end-capping agent EPPETA, as can be observed from the chromatogram (Figure S1, gray line). Although no GPC data are available for the ECA of UPEG-6-ws (i.e., PETA), the theoretical molar mass for PETA (298.3 g mol^{-1}) corresponds to the molar mass range of the byproduct visible in the chromatogram of nonpurified UPEG-6-ws. These byproducts comprising multiacrylate ECAs were removed successfully via dialysis (72 h in acetone) as shown in blue and red solid lines.

3.1.3. Evaluation of Photo-Cross-Linking Kinetics. Curing characteristics of photocurable resins are important criteria for lithography-based applications.[33] The resins should ideally show high double bond conversion and be concomitant with short processing times. To determine the photo-cross-linking kinetics of the urethane-based prepolymers at 20 °C, they were characterized via differential photocalorimetry (DPC). At 20 °C, the prepolymers are semicrystalline solids, as determined via conventional differential scanning calorimetry (Figure S2).

The cross-linking reaction of semicrystalline difunctional urethane-based PEGs was already investigated in earlier studies.[27,30,34] At room temperature, these prepolymers undergo phase separation leading to the formation of semicrystalline (PEG-rich) domains along with acrylate-rich zones. Upon exposure to UV light, free-radical polymerization propagates rapidly by reaction diffusion across the acrylate-enriched zones in the periphery of the crystalline domains. In this process, the spacer groups (i.e., six EO units) linking the acrylate moieties to the PEG-urethane backbone play a prominent role in the solid-state reactivity by providing additional motional freedom to the reactive sites.

In the photopolymerization kinetics, the role of spacers can be explained for both di- and multifunctional polymers as follows. In the case of difunctional polymers (UPEG-2), the six EO units are functioning as a "spacer" as they separate the acrylate groups from the rigid, semicrystalline PEG backbone, which is immobile during the photopolymerization process at

https://doi.org/10.1021/acs.biomac.1c00704
Biomacromolecules 2021, 22, 4919−4932

room temperature.[30] In the case of multifunctional analogs (i.e., UPEG-6), the spacers have the same function as described above. However, additionally, their spacers also separate the individual acrylate groups from each other, rendering the reactivity of the acrylate groups "independent" from each other. Indeed, when a macromonomer with two or more cross-linkable functionalities is incorporated into the radical chain upon free-radical polymerization, it is initially linked to the chain through the reaction of one double bond. The remaining double bonds hang off the network and are referred to as "pendant double bonds". The reactivity of the pendant acrylate double bonds is strongly dependent on the length and the nature of the spacing units that separate them from the previously reacted double bond. For instance, if two double bonds are connected by a rigid spacer, then their motion will be coupled, and hence, the reactivity of the pendant double bond will be reduced by the previously reacted double bond(s). If they are separated by a flexible spacer, then their individual reactivities will be independent from each other.[35−37]

As observed in Figure 3, DPC analysis revealed different reactivity trends for the prepolymers UPEG-2, UPEG-6, and UPEG-6-ws. When the prepolymers were exposed to UV radiation, immediate autoacceleration was observed according to the transient behavior toward a steady state for the photo-cross-linking of semicrystalline solids or liquids with a significant viscosity.[27] The prepolymers having a larger number of acrylates showed slower rates throughout the polymerization process. The decreasing trend in polymerization rates is likely due to the length of spacer groups. In a previous study, it was observed that the length and the chemical nature of the spacing units determine the photopolymerization rate in the semi-crystalline state.[30] More specifically, longer and less stiff spacer groups increase the polymerization rate in the semicrystalline state, and six EO units were found to be an effective spacer group that promotes the reaction of the double bonds. Considering that the spacer length of the prepolymers (Figure 1) is ranked as UPEG-2 > UPEG-6 > UPEG-6-ws, the observed trend in the polymerization rates in the semicrystalline state was anticipated. None of the prepolymers achieved full conversion likely as a result of caging or local vitrification.[27] Yet, the prepolymers with spacer groups (i.e., UPEG-2 and UPEG-6) reached a conversion of 0.80, while those lacking spacers (UPEG-6-ws) remained at a conversion of 0.53. The higher conversion of the polymers having spacer groups can be explained through the higher motional freedom of the reactive sites at room temperature. The lower final conversion as a consequence of the increased number of double bonds in the absence of spacer groups is in agreement with earlier studies reported in the literature.[33,38,39]

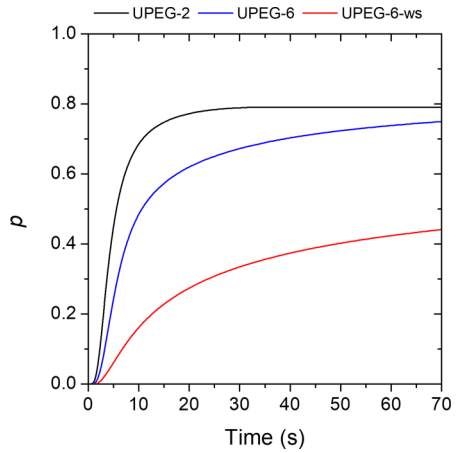

Figure 3. Conversion versus time plots of prepolymers as determined via DPC.

3.2. Characterization of the Cross-Linked Hydrogels.

Besides the photopolymerization rate, the swelling ratio and the gel fraction play an important role when designing a photo-cross-linkable polymer resin particularly for lithography-based 3D printing. After 3D printing of the photo-curable resin, it is required to wash the printed structure in a suitable solvent in order to eliminate the noncured parts (developing stage). When the structure is immersed in a solvent, the printed structure might deform as a result of extended solvent uptake. Therefore, minimizing the swelling ratio is preferable in order to eliminate the potential mismatch between the size of the implemented CAD model and the printed microstructures.

The swelling ratios and the gel fractions of the precursors are demonstrated in Figure 4a,b and Table 3. The gel fractions remained above 95% for all polymers, which is indicative of efficiently cross-linked networks irrespective of the number of double bonds or spacer units. The swelling ratios were found to be 1.8 for UPEG-2, 0.63 for UPEG-6, and 0.48 for UPEG-6-ws and were significantly different among all groups ($p < 0.05$). The decrease in the swelling ratio of the hydrogels is associated with the increasing cross-linking density. Although UPEG-6 and UPEG-6-ws have the same number of acrylates on average

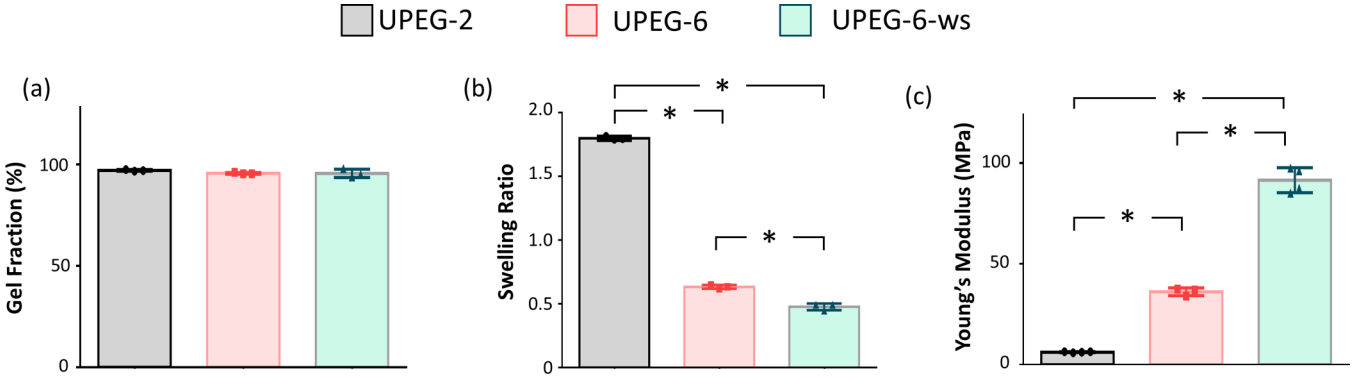

Figure 4. (a) Gel fraction, (b) swelling ratio of the UV cross-linked hydrogels, and (c) Young's modulus of the cross-linked polymers swollen to equilibrium in deionized water (*$p < 0.001$).

https://doi.org/10.1021/acs.biomac.1c00704
Biomacromolecules 2021, 22, 4919−4932

Table 3. Physical Characteristics of the Swollen Hydrogels

polymer	swelling ratio	gel fraction (%)	Young's modulus (MPa)	elongation at break (%)	deformation energy (kJ m^{-3})
UPEG-2	1.80 ± 0.02	97.1 ± 0.4	6.3 ± 0.2	12.6 ± 1.0	48.8 ± 23.5
UPEG-6	0.63 ± 0.02	95.6 ± 2.1	36.2 ± 1.9	6.0 ± 2.0	66.1 ± 38.1
UPEG-6-ws	0.48 ± 0.03	95.6 ± 0.4	91.5 ± 6.1	3.5 ± 1.2	52.7 ± 31.2

per polymer chain, the overall acrylate concentration for UPEG-6 is lower due to the presence of the spacer groups, leading to a lower density of the cross-links after UV-cross-linking and hence a higher swelling ratio compared to its counterparts lacking spacer units.

The mechanical properties of the cross-linked polymers were determined using a universal tensile tester. Prior to tensile testing, the hydrogels were swollen to equilibrium by incubation in deionized water for 24 h. The Young's modulus of UPEG-2 was found to be comparable to those of the hydrated PEGDA (700 g mol^{-1}) networks (2−10 MPa) that are frequently applied in 2PP applications (Table 3).[22] As observed in Figure 4c and Table 3, the increased number of double bonds resulted in polymer networks with substantially higher stiffness (6-fold for UPEG-6 and 14-fold for UPEG-6-ws). Considering that the increase in the acrylate groups was only 2.5-fold for UPEG-6 and 3.5-fold for UPEG-6-ws compared to UPEG-2 (Table 2), the stiffness was not observed to be proportional to the cross-linking density of the hydrogels. The substantially higher Young's moduli of UPEG-6 and UPEG-6-ws are likely a result of phase separation occurring between the rigid polyacrylate segments and the soft PEG segments, as explained in an earlier study.[26] This is potentially beneficial for high-resolution 3D printing applications due to the formation of networks with higher load-bearing capacity and hence an increased stiffness of small parts and features.[40] It was evidenced that the increase in the acrylate groups resulted in a trade-off between the stiffness and the elongation at break (Figure S3). Lower elongation at break values were observed for the multifunctional polymers UPEG-6 and UPEG-6-ws compared to UPEG-2. However, no significant difference was observed between the deformation energies of the three different hydrogels, indicating that the toughness was not affected significantly (Table 3).

3.3. Cell Culture Tests. One of the essential characteristics of an ideal tissue engineering scaffold is having no adverse effect on cell viability such as cytotoxicity. In order to assess the cytocompatibility of the developed hydrogels in the current study, we performed an indirect cell culture assay according to the ISO 10993-5 standard protocol.

The relative metabolic activities of the human foreskin fibroblasts (HFFs) cultured in the extract media of the hydrogels are shown in Figure 5. It was observed that the relative metabolic activity of the cells cultured in the sample extracts was not significantly lower compared to the control group, indicating that no toxic leachable compounds are released into the media from the cross-linked hydrogels.

Besides cytocompatibility, a tissue engineering scaffold should ideally provide good cell−material interactions in order to enable tissue growth. However, the protein-repellent character of most of the synthetic hydrogels restricts their interaction with living cells. A common strategy to introduce cell-interactive properties on synthetic biomaterials is the covalent or physical immobilization of proteins derived from the extracellular matrix (ECM).[41] Over the past decades, gelatin derivatives have attracted considerable attention in

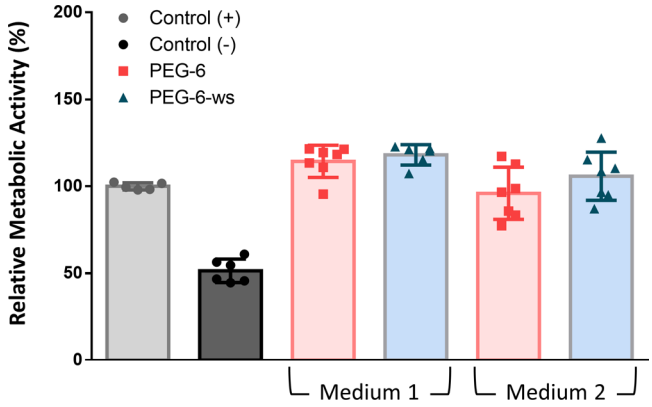

Figure 5. Relative metabolic activity of human foreskin fibroblasts (HFFs) cultured in the extract media of PEG-6 and PEG-6-ws hydrogel disks for 24 h according to ISO 10993-5. Medium 1 corresponds to culture medium extract, whereas Medium 2 corresponds to the culture medium supplemented with 0.5 vol % DMSO extract. Control (+) is the extract-free cell culture medium, and Control (−) is the culture medium supplemented with 10 vol % DMSO.

tissue engineering applications.[42] This is because gelatin is inexpensive and biodegradable and it retains natural cell binding sites such as arginine-glycine-aspartic acid (RGD), which is the most common motif responsible for cell adhesion. In previous studies concerned with the production of cell-interactive scaffolds, gelatin derivatives have already been incorporated into PEG-based matrices often through bulk modification.[43−46] In the current work, the hydrogels were coated with a methacrylated gelatin formulation (X Gel-MA INX) to improve the cell-interactive properties as schematically represented in Figure 6a. In order to ensure a homogeneous coating, the hydrogels were treated with argon plasma to introduce functional groups on the surface prior to dip-coating with X Gel-MA INX. Next, the potential applicability of the newly developed hydrogels in the tissue engineering field was evaluated by seeding human foreskin fibroblasts (HFF) onto the cross-linked hydrogel films.

Fluorescence microscopy images of HFFs seeded onto hydrogels with and without coating are presented in Figure 6b. After 7 days, a very low cell density was observed on the noncoated hydrogels. Particularly, the cells seeded on UPEG-6 hydrogels revealed a round morphology, in contrast to a more spread morphology for those cultured on UPEG-6-ws hydrogels as observed qualitatively. The latter can be related to the presence of PO spacer groups in UPEG-6 molecules, which makes these hydrogels more hydrophobic, thereby restricting protein adhesion. Nevertheless, the improvement in the cell adhesion on both hydrogels was remarkable when the samples were coated with the X Gel-MA INX formulation prior to cell culture. The cells formed a confluent monolayer after 7 days on both surface-functionalized UPEG-6 and UPEG-6-ws. The MTS assay revealed a significantly higher metabolic activity of the cells cultured on the coated hydrogels

https://doi.org/10.1021/acs.biomac.1c00704
Biomacromolecules 2021, 22, 4919−4932

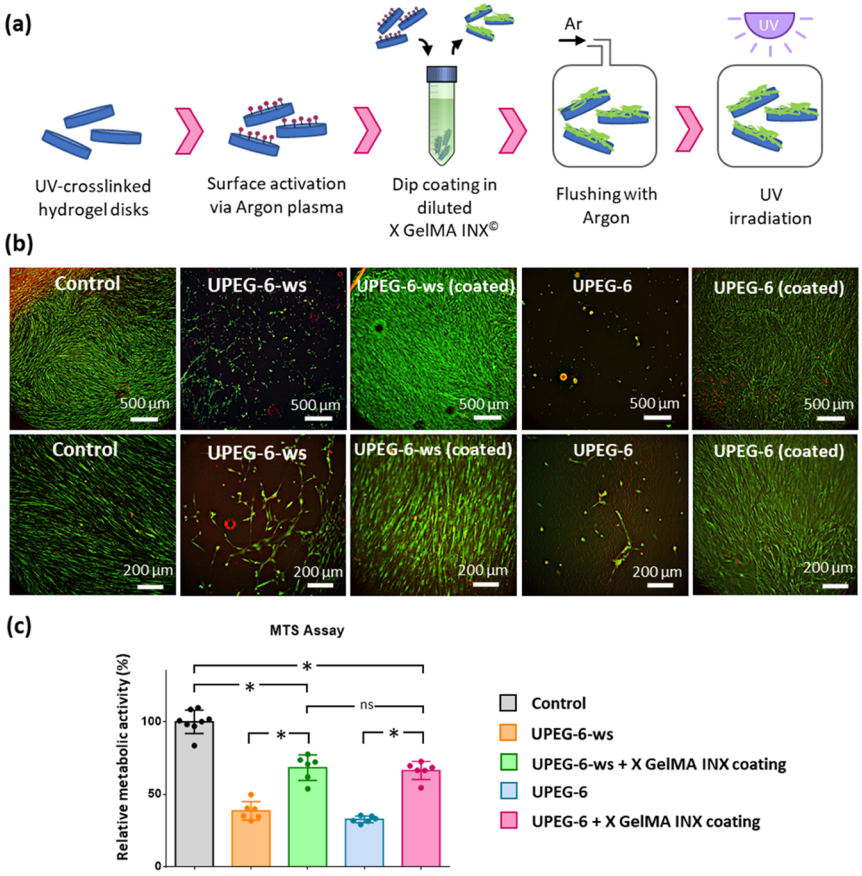

Figure 6. (a) Schematic representation of the surface functionalization of hydrogel disks using a diluted X Gel-MA INX solution. (b) Fluorescence microscopy images of HFF cells cultured on UPEG-6 and UPEG-6-ws films with and without the X Gel-MA INX coating and a tissue culture plate (control) after staining with calcein AM/propidium iodide on the seventh day of the culture and (c) relative metabolic activity of HFFs cultured on hydrogel disks (normalized according to the control group) on the seventh day of culture as determined via MTS analysis. *$p < 0.001$, and ns represents no statistically significant difference.

compared to those without coating (Figure 6c). No significant difference was observed between the metabolic activities of the cells seeded on coated UPEG-6 and UPEG-6-ws ($p > 0.05$).

PEG derivatives are known to exhibit an effective protein-repellent activity due to their hydrophilicity, high surface mobility, and steric stabilization effects.[47] Inhibition of the protein adhesion onto PEG-based surfaces leads to a reduction in cell attachment because most of the cell interactions are protein-mediated.[48] Due to the protein-repellent character of PEG derivatives, these materials have already been applied for providing selective cell−material interactions upon binding growth factors onto inert PEG matrices.[49,50] In order to increase cell adhesion, PEG derivatives are often combined with ECM proteins like heparin, hyaluronic acid, collagen, and gelatin.[51] Addition of acrylic acid into the PEGDA formulations has also been reported to improve protein adsorption as a result of the negatively charged hydrogel due to the free carboxylic acid groups.[52] Therefore, PEG-based materials can be used for controlling cell−material interactions by preventing or facilitating specific cell adhesion.[9] PEG-based formulations have successfully been applied in 2PP fabrication in earlier studies with the use of various cell types including intestinal cells,[52] fibroblasts,[53] vascular smooth muscle-like cells,[9] endothelial cells,[25,52] and neuronal cells.[23]

The direct and/or indirect cell culture tests performed with the use of fibroblasts and HepG2 cells (Figure S4) revealed no adverse effect on the metabolic activity of the applied cells, suggesting the compatibility of the newly developed hydrogels with biological applications. In particular, for tissue engineering applications, cell interactions can be facilitated by the application of a gelatin-based surface coating. Application of a post-processing surface coating on the hydrogels is potentially applicable for 2PP-manufactured microscale scaffolds, as bulk modification of the resin prior to 2PP structuring could potentially alter the processing potential, leading to microstructures with poor shape fidelity.

3.4. Evaluation of the Two-Photon Polymerization (2PP) Performance. One of the essential requirements for tissue engineering scaffolds is the design of interconnective porous structures that requires complex architectures with an open geometry of the walls. However, porous structures printed via 2PP are more prone to deformation compared to bulky structures, known to be caused by capillary forces induced by the surface tension of the evaporating developer.[15] Moreover, "freestanding" parts in the printed structures are prone to structural deformations and eventual collapse in the case of complex scaffold architectures. Therefore, it is challenging to obtain stable microstructures with complex architectures using current hydrogel precursors that form loosely cross-linked networks. The novel hydrogels based on hexafunctional precursors have a lower swelling ratio and higher stiffness as a result of the higher cross-linking density compared to their difunctional counterparts. These features characterizing the hexafunctional polymers were hypothesized

https://doi.org/10.1021/acs.biomac.1c00704
Biomacromolecules 2021, 22, 4919−4932

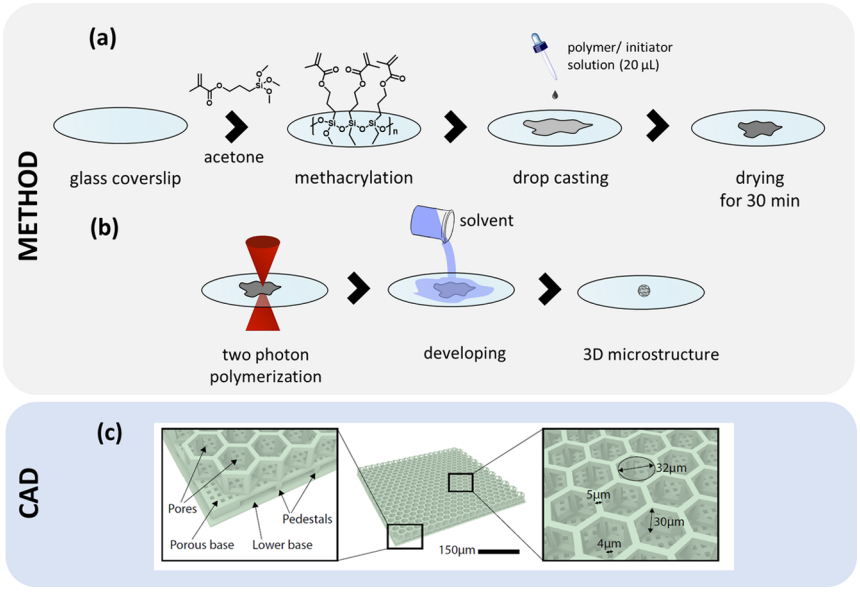

Figure 7. Schematic representation for 3D microstructuring of polymers via 2PP: (a) sample preparation, (b) microstructuring, and (c) CAD model of the microscaffolds.

to have a positive impact on the 2PP performance due to the increased stability of the printed microstructures.

The practical steps applied for the 2PP process are represented schematically in Figure 7a,b. In brief, the polymer/photoinitiator solution was drop cast onto a presilanized glass coverslip, kept at room temperature for 30 min in order to enable the evaporation of THF, and subsequently processed via 2PP at room temperature. After the processing step, the glass coverslips were soaked into a solvent to remove the nonilluminated precursors (developing stage). The 2PP potential of the hydrogel precursors was explored by printing small- (85 μm × 85 μm) and larger-scale (500 μm × 500 μm) microscaffolds using the same parameter range (5−50 mW for laser power and 10−90 mm s^{-1} for scanning speed) and the computer-aided design (CAD) model as shown in Figure 7c.

SEM images of the small-scale microscaffolds fabricated using UPEG-2, UPEG-6, and UPEG-6-ws are shown in Figure 8d−g. The increased number of double bonds clearly had a positive impact on 2PP processing. The microstructures printed using UPEG-2 exhibited significant post-processing deformation (Figure 8a), whereas those from multifunctional polymers revealed a nearly excellent CAD-CAM mimicry with no visible deformation on the porous plate nor on the honeycomb-shaped pores (Figure 8b,c). The dimensions of the pores in the porous base were found to be somewhat lower than the theoretical values for all polymers with total deformations of 29, 18, and 28% on average for UPEG-2, UPEG-6, and UPEG-6-ws, respectively. On the other hand, the differences in deformations between the different polymers were observed to be more prominent in the size of the honeycomb pores, which were found to be 43.3, 2.8, and 8.2% for UPEG-2, UPEG-6, and UPEG-6-ws, respectively. The scaffolds printed using multifunctional polymers resulted in a more uniform distribution of pore sizes compared to those of UPEG-2 as shown in the histograms in Figure S5. Successful printing of a scaffold with larger dimensions (500 μm × 500 μm) using a 25× objective shows the possibility toward upscaling (Figure 8d,e) within reasonable processing times (15 min). It should be noted that the larger-scale structures were obtained using a scanning speed of 20 mm s^{-1}, but with the use of higher scanning speeds, the scaffolds can potentially become manufactured within a shorter time frame.

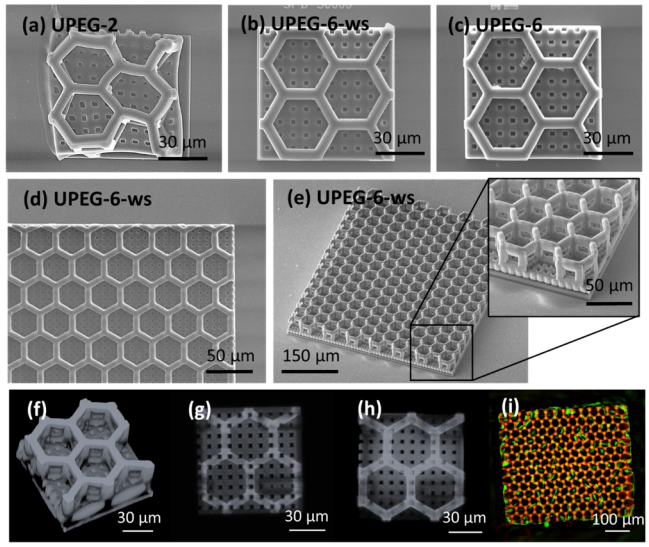

Figure 8. (a−c) SEM images of small-scale microscaffolds (85 μm × 85 μm area) fabricated using a 63× objective, (d,e) larger-scale (500 μm × 500 μm area) UPEG-6-ws microscaffold printed using a 25× objective, (f−h) confocal microscopy images of the UPEG-6-ws microscaffold in dry (f,g) and hydrated states after being incubated in PBS at 37 °C (h), and (i) fluorescence microscopy image of HFF cells cultured on a 500 μm × 500 μm scaffold on the seventh day.

The hexafunctional hydrogel precursors could be processed at scanning speeds up to 90 mm s^{-1} without a notable deformation (Figure S6). This writing speed was nearly the current limit of the experimental setup used herein, and hence, the polymers can be potentially processed at higher speeds. In the case of difunctional precursors, the microstructures revealed deformation in these processing parameters with no visible difference in the morphology.

https://doi.org/10.1021/acs.biomac.1c00704
Biomacromolecules 2021, 22, 4919−4932

In the next step, we evaluated the morphologies of the UPEG-6-ws microscaffolds after incubation in PBS at physiological temperature for 1 h. As anticipated, incubation of the UPEG-6-ws microscaffolds in PBS did not lead to deformation of the microstructures. Furthermore, the limited swelling behavior of the cross-linked UPEG-6-ws did not lead to a remarkable difference in the strut/pore dimensions (Figure S7).

To further evaluate the biocompatibility of the hydrogels after processing via 2PP, HFF cells were seeded onto the printed microscaffolds of UPEG-6-ws, and their morphology was evaluated via fluorescence microscopy after staining with calcein AM/propidium iodide. Similar to the hydrogel disks, the microscaffolds were functionalized using a five times diluted X Gel-MA INX (Xpect INX) prior to cell seeding. The HFF cells adhered onto the UPEG-6-ws microscaffolds and revealed a stretched morphology as observed on the seventh day of culture (Figure 8i), making the suggested hydrogel precursors good candidates for the fabrication of accurate structures to aid biological applications.

These proof-of-concept studies revealed that the multifunctional polymers outperformed the conventional difunctional analogs and that they are processable via 2PP at high scanning speeds to produce complex and stable 3D microstructures. Their relatively high cross-linking density owing to the high initial acrylate concentration (>1.41 mmol g^{-1}) leads to the formation of hydrogels with a higher stiffness (Young's modulus of >36 MPa) and a lower swelling ratio (<0.7), which can be considered as an advantage to produce highly stable microstructures with excellent CAD-CAM mimicry. The mechanical properties of the microscaffolds can potentially be further modulated by tuning the laser power, writing speed, and layer distance as proposed by Gou et al[22] in order to fabricate substrates with suitable mechanical properties for different cell types. Design of a telechelic polymer possessing multiple acrylate functionalities can thus be proposed as an alternative solution for the earlier reported shrinkage or swelling-related deformations in microscaffolds produced using conventional PEG formulations (e.g., PEGDA).[9,19,25] Given the highly accurate production of biocompatible microscaffolds using multifunctional hydrogel precursors, these polymers offer not only an artificial ECM for tissue growth but also a reproducible model for *in vitro* evaluation of cell behavior in 3D after application of a suitable coating for favoring the cell–material interactions.[9]

Another advantage offered by the multifunctional telechelic polymers related to 2PP processing is their excellent processability even in the absence of a solvent. The use of bulk polymers without the use of a solvent provides a higher viscosity, which has several benefits on the processing performance. On the one hand, a high viscosity is desirable for avoiding drag effects on the resin as a result of the acceleration and deceleration of the stage at turning points.[54] On the other hand, it has a potential benefit for the photopolymerization kinetics by resulting in a marked autoaccelerating effect, thereby reducing the processing times. Indeed, in a study published by Zandrini et al., it was reported that higher viscosities are favorable to having a large processability window thanks to the lower achievable polymerization thresholds.[54] As investigated earlier, the polymers developed in this study can be cross-linked in bulk with sufficiently high gel fractions (>95%), resulting in insoluble and strong gels.

Despite the above-mentioned benefits, solvent-free 2PP processing of high-molar-mass polymers comes at a cost in terms of controlling the structure dimensions. When the materials are solid-like or highly viscous melts, the 2PP process must be applied in the "oil-immersion" mode. In this mode, the laser beam is focused from the bottom of the glass substrate through an immersion oil. However, this method limits the maximum achievable structure heights due to the limited working distance and the laser focusing aberrations due to a refractive index mismatch. As a result, the maximum achievable structure height is typically in the order of tens of micrometers.[55] Considering that larger structures are required for characterization purposes and for final applications, this is one of the main challenges to be addressed when processing the newly developed polymers. To overcome this problem, the materials can be processed in the "dip-in" mode, during which the objective is directly immersed inside the precursor solution enabling the manufacturing of mesoscale structures.[55] In addition to superior control on the structure dimensions, this method allows the use of any type of substrate, which does not necessarily need to be transparent. The latter is potentially beneficial for direct printing of the microstructures onto substrates other than glass, such as silicon microfluidic chips or a prefabricated macroscale scaffold. However, only liquid precursors with controlled viscosities can be printed via the dip-in method to permit unimpeded movement of the optical components inside the precursor.[56] To this end, the hydrogel precursors can be dissolved in water or buffer rather than processing them in the solid or molten state. By dissolving the precursors in buffer, the polymers can potentially be processed in the presence of living cells for the manufacturing of cell-laden constructs.[57] The printing potential through the dip-in method is interesting from the perspective of final application. However, potential consequences with regard to photopolymerization kinetics and the stability of the final structures should be investigated in a future research study.

In general, the proposed multifunctional telechelic urethane-based PEGs showed an excellent performance for the manufacturing of stable 3D microstructures via the 2PP technology compared to their difunctional counterparts that are not compatible with the technique. The possibility to produce microstructures with high accuracy using the novel biocompatible hydrogel building blocks opens opportunities in many fields including tissue engineering, lab-on-a-chip, drug delivery systems, and drug screening applications.

4. CONCLUSIONS

Urethane-based hydrogel precursors possessing multiple acrylate functionalities on each chain end were synthesized and characterized in terms of their physicochemical characteristics, biocompatibility, and 2PP processing potential while comparing their characteristics with a difunctional analog. It was observed that increasing the number of double bonds is an elegant approach to support the 2PP fabrication of microstructures. The superior physical properties of the cross-linked multifunctional hydrogel precursors such as decreased water uptake capacity and increased physical strength can be considered key factors behind their superior processability.

All precursors investigated herein were cross-linkable at room temperature in solvent-free conditions, revealing a photopolymerization rate dependent on the number of acrylates and spacer groups present. Introducing alkoxy spacer units provided an enhanced motional freedom to the reactive

https://doi.org/10.1021/acs.biomac.1c00704
Biomacromolecules 2021, 22, 4919−4932

double bonds, thereby increasing the photopolymerization rate as well as the double bond conversion. Nevertheless, both multifunctional precursors showed an excellent 2PP processability irrespective of the presence of spacer groups, resulting in an excellent CAD-CAM mimicry at high scanning speeds up to at least 90 mm s^{-1}. Although the limited conversion of acrylates (50−80% as determined via DPC studies) in the solid state can be considered a potential drawback for biomedical applications due to the potential cytotoxic effect of the residual acrylates, all hydrogels investigated in this study were biocompatible as evidenced via cell culture assays. After application of a gelatin methacrylamide-based coating, the hydrogel films and microscaffolds revealed good cell adhesion and high viability, which are necessary for biological applications.

The development of the hexafunctional hydrogel precursors offers a solvent-free and one-pot synthesis that can potentially be applied on an industrial scale. Given their straightforward synthesis, biocompatibility, and improved processing potential, the suggested hydrogel precursors are good alternatives for the manufacturing of accurate microstructures to aid biological applications.

■ ASSOCIATED CONTENT

Supporting Information

The Supporting Information is available free of charge at https://pubs.acs.org/doi/10.1021/acs.biomac.1c00704.

> Gel permeation chromatography and differential scanning calorimetry data, indirect cytotoxicity tests using HepG2 cells, feature sizes of the manufactured microscaffolds, and SEM images of the microscaffolds that were printed at varying scanning speeds (PDF)

■ AUTHOR INFORMATION

Corresponding Authors

Sandra Van Vlierberghe − *Polymer Chemistry & Biomaterials Research Group, Centre of Macromolecular Chemistry (CMaC), Ghent University, 9000 Ghent, Belgium; Brussels Photonics (B-PHOT), Vrije Universiteit Brussel and Flanders Make, 1050 Brussels, Belgium;* orcid.org/0000-0001-7688-1682; Email: sandra.vanvlierberghe@ugent.be

Peter Dubruel − *Polymer Chemistry & Biomaterials Research Group, Centre of Macromolecular Chemistry (CMaC), Ghent University, 9000 Ghent, Belgium;* Email: peter.dubruel@ugent.be

Authors

Aysu Arslan − *Polymer Chemistry & Biomaterials Research Group, Centre of Macromolecular Chemistry (CMaC), Ghent University, 9000 Ghent, Belgium;* orcid.org/0000-0001-6153-8558

Koen Vanmol − *Brussels Photonics (B-PHOT), Vrije Universiteit Brussel and Flanders Make, 1050 Brussels, Belgium*

Agnes Dobos − *Polymer Chemistry & Biomaterials Research Group, Centre of Macromolecular Chemistry (CMaC), Ghent University, 9000 Ghent, Belgium*

Alessandra Natale − *Department of In Vitro Toxicology and Dermato-Cosmetology (IVTD), Vrije Universiteit Brussel, 1090 Brussels, Belgium*

Jasper Van Hoorick − *Polymer Chemistry & Biomaterials Research Group, Centre of Macromolecular Chemistry (CMaC), Ghent University, 9000 Ghent, Belgium*

Patrice Roose − *Allnex Belgium SA/NV, 1620 Brussels, Belgium;* orcid.org/0000-0003-2768-701X

Hugues Van den Bergen − *Allnex Belgium SA/NV, 1620 Brussels, Belgium*

Tatevik Chalyan − *Brussels Photonics (B-PHOT), Vrije Universiteit Brussel and Flanders Make, 1050 Brussels, Belgium*

Aleksandr Ovsianikov − *3D Printing and Biofabrication Group, Institute of Materials Science and Technology, TU Wien, 1060 Vienna, Austria*

Stefan Baudis − *Institute of Applied Synthetic Chemistry, TU Wien, Vienna 1060, Austria;* orcid.org/0000-0002-5390-0761

Vera Rogiers − *Department of In Vitro Toxicology and Dermato-Cosmetology (IVTD), Vrije Universiteit Brussel, 1090 Brussels, Belgium*

Tamara Vanhaecke − *Department of In Vitro Toxicology and Dermato-Cosmetology (IVTD), Vrije Universiteit Brussel, 1090 Brussels, Belgium*

Robim M. Rodrigues − *Department of In Vitro Toxicology and Dermato-Cosmetology (IVTD), Vrije Universiteit Brussel, 1090 Brussels, Belgium*

Hugo Thienpont − *Brussels Photonics (B-PHOT), Vrije Universiteit Brussel and Flanders Make, 1050 Brussels, Belgium*

Jürgen Van Erps − *Brussels Photonics (B-PHOT), Vrije Universiteit Brussel and Flanders Make, 1050 Brussels, Belgium*

Complete contact information is available at: https://pubs.acs.org/10.1021/acs.biomac.1c00704

Author Contributions

The manuscript was written through contributions of all authors. All authors have given approval to the final version of the manuscript.

Notes

The authors declare no competing financial interest.

■ ACKNOWLEDGMENTS

Financial support by the Research Foundation Flanders (FWO, Belgium) was gratefully acknowledged (research grant G030217N), as well as Interreg Vlaanderen-Nederland "Fotonica pilootlijnen", Methusalem, IOF, and OZR of Vrije Universiteit Brussel.

■ ABBREVIATIONS

2PP two-photon polymerization
$Đ$ polydispersity index
$\Delta H°$ molar reaction enthalpy
ΔH total reaction enthalpy
AM acetoxymethyl
C_{acr} acrylate concentration
CAD computer-aided design
CAM computer-aided manufacturing
DMSO dimethyl sulfoxide
DMT dimethyl terephthalate
DPC differential photocalorimetry
ECA endcapping agent
ECM extracellular matrix

EO ethylene oxide
EPPETA ethoxylated and propoxylated pentaerythritol triacrylate
FTIR Fourier transform infrared
HFF human foreskin fibroblasts
h_{max} maximum heat flow
IPDI isophorone diisocyanate
M_n number average molar mass
M_w weight average molar mass
MTS 3-(4,5-dimethylthiazol-2-yl)-5-(3-carboxymethoxyphenyl)-2-(4-sulfophenyl)-2*H*-tetrazolium
NMR nuclear magnetic resonance
n_{acr} theoretical acrylate number
OEOA oligoethyleneoxide monoacrylate
PCL poly-ϵ-caprolactone
PEG poly(ethylene glycol)
PEGDA polyethylene glycol diacrylate
PETA pentaerythritol triacrylate
PI propidium iodide
PO propylene oxide
p_f final fractional acrylate conversion
R_{max} maximum polymerization rate
UV-A ultraviolet ($315 < \lambda < 400$ nm)
UV-C ultraviolet ($200 < \lambda < 280$ nm)

REFERENCES

(1) Applegate, M. B.; Coburn, J.; Partlow, B. P.; Moreau, J. E.; Mondia, J. P.; Marelli, B.; Kaplan, D. L.; Omenetto, F. G. Laser-Based Three-Dimensional Multiscale Micropatterning of Biocompatible Hydrogels for Customized Tissue Engineering Scaffolds. *Proc. Natl. Acad. Sci. U. S. A.* **2015**, *112*, 12052−12057.

(2) Ovsianikov, A.; Malinauskas, M.; Schlie, S.; Chichkov, B.; Gittard, S.; Narayan, R.; Löbler, M.; Sternberg, K.; Schmitz, K. P.; Haverich, A. Three-Dimensional Laser Micro- and Nano-Structuring of Acrylated Poly(Ethylene Glycol) Materials and Evaluation of Their Cytoxicity for Tissue Engineering Applications. *Acta Biomater.* **2011**, *7*, 967−974.

(3) Zhang, A. P.; Qu, X.; Soman, P.; Hribar, K. C.; Lee, J. W.; Chen, S.; He, S. Rapid Fabrication of Complex 3D Extracellular Microenvironments by Dynamic Optical Projection Stereolithography. *Adv. Mater.* **2012**, *24*, 4266−4270.

(4) Hutmacher, D. W.; Sittinger, M.; Risbud, M. V. Scaffold-Based Tissue Engineering: Rationale for Computer-Aided Design and Solid Free-Form Fabrication Systems. *Trends Biotechnol.* **2004**, *22*, 354−362.

(5) Dorfinger, P.; Stampfl, J.; Liska, R. Toughening of Photopolymers for Stereolithography (SL). *Mater. Sci. Forum* **2015**, *825-826*, 53−59.

(6) Orman, S.; Hofstetter, C.; Aksu, A.; Reinauer, F.; Liska, R.; Baudis, S. Toughness Enhancers for Bone Scaffold Materials Based on Biocompatible Photopolymers. *J. Polym. Sci. Part A Polym. Chem.* **2019**, *57*, 110−119.

(7) Tian, H.; Tang, Z.; Zhuang, X.; Chen, X.; Jing, X. Biodegradable Synthetic Polymers: Preparation, Functionalization and Biomedical Application. *Prog. Polym. Sci.* **2012**, *37*, 237−280.

(8) Place, E. S.; George, J. H.; Williams, C. K.; Stevens, M. M. Synthetic Polymer Scaffolds for Tissue Engineering. *Chem. Soc. Rev.* **2009**, *38*, 1139−1151.

(9) Ovsianikov, A.; Gruene, M.; Pflaum, M.; Koch, L.; Maiorana, F.; Wilhelmi, M.; Haverich, A.; Chichkov, B. Laser Printing of Cells into 3D Scaffolds. *Biofabrication* **2010**, *2*, No. 014104.

(10) Torgersen, J.; Qin, X.-H.; Li, Z.; Ovsianikov, A.; Liska, R.; Stampfl, J. Hydrogels for Two-Photon Polymerization: A Toolbox for Mimicking the Extracellular Matrix. *Adv. Funct. Mater.* **2013**, *23*, 4542−4554.

(11) Gittard, S. D.; Ovsianikov, A.; Akar, H.; Chichkov, B.; Monteiro-Riviere, N. A.; Stafslien, S.; Chisholm, B.; Shin, C. C.; Shih, C. M.; Lin, S. J.; et al. Two Photon Polymerization-Micromolding of Polyethylene Glycol-Gentamicin Sulfate Microneedles. *Adv. Eng. Mater.* **2010**, *12*, 77−82.

(12) Lasagni, A. F.; Yuan, D.; Shao, P.; Das, S. Periodic Micropatterning of Polyethylene Glycol Diacrylate Hydrogel by Laser Interference Lithography Using Nano-and Femtosecond Pulsed Lasers. *Adv. Eng. Mater.* **2009**, *11*, 20−24.

(13) Scarpa, E.; Lemma, E. D.; Fiammengo, R.; Cipolla, M. P.; Pisanello, F.; Rizzi, F.; De Vittorio, M. Microfabrication of PH-Responsive 3D Hydrogel Structures via Two-Photon Polymerization of High-Molecular-Weight Poly(Ethylene Glycol) Diacrylates. *Sens. Actuators, B* **2019**, *279*, 418−426.

(14) Wloka, T.; Czich, S.; Kleinsteuber, M.; Moek, E.; Weber, C.; Gottschaldt, M.; Liefeith, K.; Schubert, U. S. Microfabrication of 3D-Hydrogels via Two-Photon Polymerization of Poly(2-Ethyl-2-Oxazoline) Diacrylates. *Eur. Polym. J.* **2020**, *122*, 109295.

(15) Käpylä, E.; Sedlačík, T.; Aydogan, D. B.; Viitanen, J.; Rypáček, F.; Kellomäki, M. Direct Laser Writing of Synthetic Poly(Amino Acid) Hydrogels and Poly(Ethylene Glycol) Diacrylates by Two-Photon Polymerization. *Mater. Sci. Eng. C* **2014**, *43*, 280−289.

(16) Qin, X. H.; Wang, X.; Rottmar, M.; Nelson, B. J.; Maniura-Weber, K. Near-Infrared Light-Sensitive Polyvinyl Alcohol Hydrogel Photoresist for Spatiotemporal Control of Cell-Instructive 3D Microenvironments. *Adv. Mater.* **2018**, *30*, 1−7.

(17) Berg, A.; Wyrwa, R.; Weisser, J.; Weiss, T.; Schade, R.; Hildebrand, G.; Liefeith, K.; Schneider, B.; Ellinger, R.; Schnabelrauch, M. Synthesis of Photopolymerizable Hydrophilic Macromers and Evaluation of Their Applicability as Reactive Resin Components for the Fabrication of Three-Dimensionally Structured Hydrogel Matrices by 2-Photon-Polymerization. *Adv. Eng. Mater.* **2011**, *13*, B274−B284.

(18) Tessmar, J. K.; Göpferich, A. M. Customized PEG-Derived Copolymers for Tissue-Engineering Applications. *Macromol. Biosci.* **2007**, *7*, 23−39.

(19) Klein, F.; Richter, B.; Striebel, T.; Franz, C. M.; Von Freymann, G.; Wegener, M.; Bastmeyer, M. Two-Component Polymer Scaffolds for Controlled Three-Dimensional Cell Culture. *Adv. Mater.* **2011**, *23*, 1341−1345.

(20) Park, S.-H.; Kim, K. H.; Lim, T. W.; Yang, D.-Y.; Lee, K.-S. Investigation of Three-Dimensional Pattern Collapse Owing to Surface Tension Using an Imperfection Finite Element Model. *Microelectron. Eng.* **2008**, *85*, 432−439.

(21) Xing, J.; Liu, L.; Song, X.; Zhao, Y.; Zhang, L.; Dong, X.; Jin, F.; Zheng, M.; Duan, X. 3D Hydrogels with High Resolution Fabricated by Two-Photon Polymerization with Sensitive Water Soluble Initiators. *J. Mater. Chem. B* **2015**, *3*, 8486−8491.

(22) Gou, X.; Zheng, M.; Zhao, Y.; Dong, X.; Jin, F.; Xing, J.; Duan, X. Mechanical Property of PEG Hydrogel and the 3D Red Blood Cell Microstructures Fabricated by Two-Photon Polymerization. *Appl. Surf. Sci.* **2017**, *416*, 273−280.

(23) Accardo, A.; Blatché, M.-C.; Courson, R.; Loubinoux, I.; Vieu, C.; Malaquin, L. Two-Photon Lithography and Microscopy of 3D Hydrogel Scaffolds for Neuronal Cell Growth. *Biomed. Phys. Eng. Express* **2018**, *4*, No. 027009.

(24) Hasselmann, N. F.; Hackmann, M. J.; Horn, W. Two-Photon Fabrication of Hydrogel Microstructures for Excitation and Immobilization of Cells. *Biomed. Microdevices* **2018**, *20*, 8.

(25) Nguyen, A. K.; Gittard, S. D.; Koroleva, A.; Schlie, S.; Gaidukeviciute, A.; Chichkov, B. N.; Narayan, R. J. Two-Photon Polymerization of Polyethylene Glycol Diacrylate Scaffolds with Riboflavin and Triethanolamine Used as a Water-Soluble Photoinitiator. *Regen. Med.* **2013**, *8*, 725−738.

(26) Arslan, A.; Steiger, W.; Roose, P.; Van den Bergen, H.; Gruber, P.; Zerobin, E.; Gantner, F.; Guillaume, O.; Ovsianikov, A.; Van Vlierberghe, S.; et al. Polymer Architecture as Key to Unprecedented High-Resolution 3D-Printing Performance: The Case of Biodegrad-

https://doi.org/10.1021/acs.biomac.1c00704
Biomacromolecules 2021, 22, 4919−4932

able Hexa-Functional Telechelic Urethane-Based Poly-ε-Caprolactone. *Mater. Today* **2021**, *44*, 25−39.
(27) Roose, P.; Van Den Bergen, H.; Houben, A.; Bontinck, D.; Van Vlierberghe, S. A Semiempirical Scaling Model for the Solid- and Liquid-State Photopolymerization Kinetics of Semicrystalline Acrylated Oligomers. *Macromolecules* **2018**, *51*, 5027−5038.
(28) France, R. M.; Short, R. D. Plasma Treatment of Polymers Effects of Energy Transfer from an Argon Plasma on the Surface Chemistry of Poly(Styrene), Low Density Poly(Ethylene), Poly-(Propylene) and Poly(Ethylene Terephthalate). *J. Chem. Soc. - Faraday Trans.* **1997**, *93*, 3173−3178.
(29) Ajami, A.; Husinsky, W.; Tromayer, M.; Gruber, P.; Liska, R.; Ovsianikov, A. Measurement of Degenerate Two-Photon Absorption Spectra of a Series of Developed Two-Photon Initiators Using a Dispersive White Light Continuum Z-Scan. *Appl. Phys. Lett.* **2017**, *111*, No. 071901.
(30) Houben, A.; Roose, P.; Van den Bergen, H.; Declercq, H.; Van Hoorick, J.; Gruber, P.; Ovsianikov, A.; Bontinck, D.; Van Vlierberghe, S.; Dubruel, P. Flexible Oligomer Spacers as the Key to Solid-State Photopolymerization of Hydrogel Precursors. *Mater. Today Chem.* **2017**, *4*, 84−89.
(31) Kricheldorf, H. R. Syntheses of Biodegradable and Biocompatible Polymers by Means of Bismuth Catalysts. *Chem. Rev.* **2009**, *109*, 5579−5594.
(32) Lomölder, R.; Plogmann, F.; Speier, P. Selectivity of Isophorone Diisocyanate in the Urethane Reaction Influence of Temperature, Catalysis, and Reaction Partners. *J. Coat. Technol.* **1997**, *69*, 51−57.
(33) Schuster, M.; Turecek, C.; Mateos, A.; Stampfl, J.; Liska, R.; Varga, F. Evaluation of Biocompatible Photopolymers II: Further Reactive Diluents. *Monatsh. Chem.* **2007**, *138*, 261−268.
(34) Roose, P.; Vermoesen, E.; Van Vlierberghe, S. Non-Steady Scaling Model for the Kinetics of the Photo-Induced Free Radical Polymerization of Crosslinking Networks. *Polym. Chem.* **2020**, *11*, 2475−2484.
(35) Andrzejewska, E. Photopolymerization Kinetics of Multifunctional Monomers. *Prog. Polym. Sci.* **2001**, *26*, 605−665.
(36) Andrzejewska, E. Free Radical Photopolymerization of Multifunctional Monomers. In *Three-Dimensional Microfabrication Using Two-photon Polymerization*; Elsevier, 2016; pp. 62−81, DOI: 10.1016/B978-0-323-35321-2.00004-2.
(37) Cook, W. D. Thermal Aspects of the Kinetics of Dimethacrylate Photopolymerization. *Polymer (Guildf).* **1992**, *33*, 2152−2161.
(38) Khudyakov, I. V.; Legg, J. C.; Purvis, M. B.; Overton, B. J. Kinetics of Photopolymerization of Acrylates with Functionality of 1−6. *Ind. Eng. Chem. Res.* **1999**, *38*, 3353−3359.
(39) White, T. J.; Liechty, W. B.; Guymon, C. A. The Influence of N-Vinyl Pyrrolidone on Polymerization Kinetics and Thermo-Mechanical Properties of Crosslinked Acrylate Polymers. *J. Polym. Sci. Part A Polym. Chem.* **2007**, *45*, 4062−4073.
(40) Van Hoorick, J.; Gruber, P.; Markovic, M.; Tromayer, M.; Van Erps, J.; Thienpont, H.; Liska, R.; Ovsianikov, A.; Dubruel, P.; Van Vlierberghe, S. Cross-Linkable Gelatins with Superior Mechanical Properties Through Carboxylic Acid Modification: Increasing the Two-Photon Polymerization Potential. *Biomacromolecules* **2017**, *18*, 3260−3272.
(41) Desmet, T.; Billiet, T.; Berneel, E.; Cornelissen, R.; Schaubroeck, D.; Schacht, E.; Dubruel, P. Post-Plasma Grafting of AEMA as a Versatile Tool to Biofunctionalise Polyesters for Tissue Engineering. *Macromol. Biosci.* **2010**, *10*, 1484−1494.
(42) Van Hoorick, J.; Tytgat, L.; Dobos, A.; Ottevaere, H.; Van Erps, J.; Thienpont, H.; Ovsianikov, A.; Dubruel, P.; Van Vlierberghe, S. (Photo-)Crosslinkable Gelatin Derivatives for Biofabrication Applications. *Acta Biomater.* **2019**, *97*, 46−73.
(43) Daniele, M. A.; Adams, A. A.; Naciri, J.; North, S. H.; Ligler, F. S. Interpenetrating Networks Based on Gelatin Methacrylamide and PEG Formed Using Concurrent Thiol Click Chemistries for Hydrogel Tissue Engineering Scaffolds. *Biomaterials* **2014**, *35*, 1845−1856.
(44) Gao, G.; Schilling, A. F.; Hubbell, K.; Yonezawa, T.; Truong, D.; Hong, Y.; Dai, G.; Cui, X. Improved Properties of Bone and Cartilage Tissue from 3D Inkjet-Bioprinted Human Mesenchymal Stem Cells by Simultaneous Deposition and Photocrosslinking in PEG-GelMA. *Biotechnol. Lett.* **2015**, *37*, 2349−2355.
(45) Xiao, S.; Zhao, T.; Wang, J.; Wang, C.; Du, J.; Ying, L.; Lin, J.; Zhang, C.; Hu, W.; Wang, L.; et al. Gelatin Methacrylate (GelMA)-Based Hydrogels for Cell Transplantation: An Effective Strategy for Tissue Engineering. *Stem Cell Rev. Reports* **2019**, *15*, 664−679.
(46) Wang, Z.; Abdulla, R.; Parker, B.; Samanipour, R.; Ghosh, S.; Kim, K. A Simple and High-Resolution Stereolithography-Based 3D Bioprinting System Using Visible Light Crosslinkable Bioinks. *Biofabrication* **2015**, *7*, No. 045009.
(47) Lee, J. H.; Kopecek, J.; Andrade, J. D. Protein-resistant Surfaces Prepared by PEO-containing Block Copolymer Surfactants. *J. Biomed. Mater. Res.* **1989**, *23*, 351−368.
(48) Desai, N. P.; Hubbell, J. A. Solution Technique to Incorporate Polyethylene Oxide and Other Water-Soluble Polymers into Surfaces of Polymeric Biomaterials. *Biomaterials* **1991**, *12*, 144−153.
(49) Lee, S. H.; Moon, J. J.; West, J. L. Three-Dimensional Micropatterning of Bioactive Hydrogels via Two-Photon Laser Scanning Photolithography for Guided 3D Cell Migration. *Biomaterials* **2008**, *29*, 2962−2968.
(50) Leslie-Barbick, J. E.; Shen, C.; Chen, C.; West, J. L. Micron-Scale Spatially Patterned, Covalently Immobilized Vascular Endothelial Growth Factor on Hydrogels Accelerates Endothelial Tubulogenesis and Increases Cellular Angiogenic Responses. *Tissue Eng. - Part A* **2011**, *17*, 221−229.
(51) Marchioli, G.; Zellner, L.; Oliveira, C.; Engelse, M.; de Koning, E.; Mano, J.; Karperien; van Apeldoorn, A.; Moroni, L. Layered PEGDA Hydrogel for Islet of Langerhans Encapsulation and Improvement of Vascularization. *J. Mater. Sci. Mater. Med.* **2017**, *28*, 195.
(52) Creff, J.; Courson, R.; Mangeat, T.; Foncy, J.; Souleille, S.; Thibault, C.; Besson, A.; Malaquin, L. Fabrication of 3D Scaffolds Reproducing Intestinal Epithelium Topography by High-Resolution 3D Stereolithography. *Biomaterials* **2019**, *221*, 119404.
(53) Yu, H.; Liu, J.; Zhao, Y. Y.; Jin, F.; Dong, X. Z.; Zhao, Z. S.; Duan, X. M.; Zheng, M. L. Biocompatible Three-Dimensional Hydrogel Cell Scaffold Fabricated by Sodium Hyaluronate and Chitosan Assisted Two-Photon Polymerization. *ACS Appl. Bio Mater.* **2019**, *2*, 3077−3083.
(54) Zandrini, T.; Liaros, N.; Jiang, L. J.; Lu, Y. F.; Fourkas, J. T.; Osellame, R.; Baldacchini, T. Effect of the Resin Viscosity on the Writing Properties of Two-Photon Polymerization. *Opt. Mater. Express* **2019**, *9*, 2601−2616.
(55) Bückmann, T.; Stenger, N.; Kadic, M.; Kaschke, J.; Frölich, A.; Kennerknecht, T.; Eberl, C.; Thiel, M.; Wegener, M. Tailored 3D Mechanical Metamaterials Made by Dip-in Direct-Laser-Writing Optical Lithography. *Adv. Mater.* **2012**, *24*, 2710−2714.
(56) Baldacchini, T. *Three-Dimensional Microfabrication Using Two-Photon Polymerization: Fundamentals, Technology, and Applications*; William Andrew, Elsevier, 2015.
(57) Ovsianikov, A.; Mühleder, S.; Torgersen, J.; Li, Z.; Qin, X. H.; Van Vlierberghe, S.; Dubruel, P.; Holnthoner, W.; Redl, H.; Liska, R.; et al. Laser Photofabrication of Cell-Containing Hydrogel Constructs. *Langmuir* **2014**, *30*, 3787−3794.

https://doi.org/10.1021/acs.biomac.1c00704
Biomacromolecules 2021, 22, 4919−4932